TRENDS IN SCIENCES 2025; 22(11): 10815
https://doi.org/10.48048/tis.2025.10815 RESEARCH ARTICLE

An *In Vitro* Hypoxic Cancer Model Using $CoCl_2$ on Vietnamese Breast Cancer Cells for Potential Drug Screening

Chau Nguyen Minh Hoang[2], Bui Dinh Khan[2,3], Tran Ngo The Nhan[2,3] and Pham Duy Khuong[1,2,3,*]

[1]*Laboratory of Tissue Engineering and Biomedical Materials, University of Science - VNUHCM, Ho Chi Minh, Vietnam*
[2]*Viet Nam National University, Ho Chi Minh, Vietnam*
[3]*VNUHCM-US Stem Cell Institute, University of Science, Viet Nam National University, Ho Chi Minh, Vietnam*

([*]Corresponding author's e-mail: pdkhuong@hcmus.edu.vn)

Received: 5 June 2025, Revised: 18 June 2025, Accepted: 18 June 2025, Published: 20 August 2025

Abstract

Developing effective anti-cancer drugs and overcoming drug resistance continue to pose significant challenges in cancer research and clinical practice. Despite notable advancements, existing cell culture models, including advanced 3D systems, often fall short in terms of speed, scalability, and cost-effectiveness, particularly for high-throughput screening. To address these limitations, this study introduces a simple, cost-effective hypoxia model using 250 µM cobalt (II) chloride ($CoCl_2$) in Vietnamese breast cancer cell lines (VNBRCA1) to simulate the tumor microenvironment. The induced hypoxic conditions resulted in a significant upregulation of stemness-related genes (*Nanog, Sox-4, Oct-2*), autophagy-related genes (*LC3-II, Beclin-1*), and hypoxia-related genes (*HIF-1α, HIF-2α*), as confirmed by real-time quantitative PCR (RT-qPCR). Functional assays demonstrated enhanced cell migration under hypoxia, as shown by RT-qPCR and wound healing analysis, potentially involving a hybrid epithelial-mesenchymal transition (EMT) mechanism. The model's applicability was further assessed through cisplatin treatment, revealing distinct responses under hypoxic versus normoxic conditions. These findings suggest that the $CoCl_2$-induced hypoxia system offers a practical approach to simulating tumor microenvironments, providing a reproducible and scalable *in vitro* platform for studying tumor biology and evaluating anti-cancer strategies in a more physiologically relevant context.

Keywords: Breast cancer, Cancer *in vitro* model, Hypoxia, Autophagy, Hybrid EMT, Stemness

Introduction

Cancer is one of the most devastating diseases globally, with nearly 20 million new cases diagnosed and nearly 10 million deaths by 2022. The American Cancer Society predicts that by 2050, the number of cancer cases is expected to increase to 35 million. Despite significant advances in cancer research and treatment, cancer-related deaths continue to rise [1]. A significant reason for this issue is the inability of preclinical models to accurately mimic the complexities of the tumor microenvironment. This disconnect often results in promising drug candidates failing during clinical trials, leading to a waste of time and resources. According to 1 study, pharmaceutical and biotechnology companies lose resources annually in drug discovery and testing processes that achieve success in only 5% of cases [2]. Recognizing the important role of the tumor microenvironment in cancer progression, scientists are increasingly focusing on integrating these factors into preclinical models. By integrating components of the tumor microenvironment, researchers can create more precise simulations of human cancers, thereby increasing the predictive

accuracy of these models in evaluating drug responses. Furthermore, the advancement of tumor-like models is crucial for deepening our understanding of tumor progression, metastasis, and, most importantly, drug resistance.

Several promising models have been developed for drug screening to address this issue. Among them, 2D cell cultures are still the most common method used in high-throughput drug screening due to their cost-effectiveness and ease of use [3-5]. However, 2D cell cultures have certain limitations. The 2D cell cultures fail to mimic the tumor-specific architecture, the mechanical and biochemical signals, and the cell-cell and cell-extracellular matrix (ECM) communications. As a result, they may not accurately reflect the genetic and phenotypic heterogeneity of human cancers or predict clinical efficacy and toxicity [6]. To address these limitations, researchers have developed cancer organoid models. These are 3-dimensional, self-organizing structures derived from primary tumor samples or stem cells that can recapitulate the cellular composition, architecture, and functional properties of the original tumor [7]. This allows for more physiologically relevant drug screening and personalized therapy. Despite the numerous advantages, 3D models also have downsides when compared to 2D cell models for drug screening, such as difficulties in visualization and flow cytometry analysis. Additionally, creating 3D models demands specialized expertise and equipment, leading to significant labor and expensive costs [6]. Other important disadvantages of using 3D models include the lack of affordable standard methods to develop 3D cell cultures and the right assays to test drugs with future clinical relevance, associated with the difficulty of replicating experiments and interpreting the resulting data [8]. Therefore, the use of 3D cancer models for preclinical drug screening can be challenging due to the large variability between the different models and the difficulty in combining these models with high-throughput screening (HTS) and high-content imaging (HCI) approaches [6].

To overcome these challenges, researchers are developing more sophisticated *in vitro* tumor models that better mimic the tumor microenvironment and provide more reliable drug efficacy and resistance predictions. One critical aspect of the tumor microenvironment is hypoxia—a condition of reduced oxygen availability that is common in solid tumors. In tumors, oxygen level tends to decrease gradually from the outer layers to the central core, leading to a condition termed “hypoxia” [6]. Moreover, the cancer cells are triggered to respond in hypoxic conditions through the upregulation of transcription factors, hypoxia-induced factors (*HIFs*), which play a particularly important role in tumors [9]. Many studies showed the increasing level of the expression of *HIF-1α* or *HIF-2α* to adapt to the decreased oxygen available conditions in many types of cancer cells [10]. During the adaptation to stress conditions, tumor hypoxia has been proven to induce autophagy in cancer cells [11]. Autophagy is a process in which cells transport their proteins and organelles to lysosomes for degradation in response to stress conditions [12]. In many cancers, autophagy is demonstrated as the factor that can promote tumorigenesis by assisting cancer-cell proliferation and tumor growth [13].

Moreover, hypoxia is closely linked to EMT. EMT events provide epithelial cells with increased migratory and invasive potential and, as a result, have been implicated in a variety of physiological and pathological processes involving cell migration [14]. Indeed, EMT is a critical mechanism in cancer that contributes to metastasis and is characterized by the loss of epithelial characteristics (*E-cadherin*) and the overexpression of mesenchymal properties (*Vimentin* and *N-cadherin*) [15]. EMT has recently been linked to cancer cells in several studies, especially under hypoxic conditions [16]. Furthermore, cancer stem cells or cancer cells exhibiting stem cell-like properties are also recognized for their crucial role in promoting tumor growth [17]. However, replicating this phenomenon *in vitro* poses challenges due to the heterogeneity of cancer cells, making it difficult for researchers to create a model that accurately reflects the properties of the tumor.

Hence, the development of a new hypoxia-enhanced cancer model is essential for our understanding of cancer and exploring potential treatment options. This study employs $CoCl_2$ to create hypoxic conditions in a 2D breast cancer model by increasing the expression of hypoxia-related factors and further evaluates factors associated with the tumor microenvironment comprising autophagy, stemness, and migration capabilities of the cancer cells. Moreover, the hypoxia-enhanced models are utilized to evaluate

drug responses in comparison to traditional culture models. This research holds the potential to transform oncology, paving the way for more effective treatments with reduced side effects. By leveraging cutting-edge technology and building upon existing knowledge, we aim to develop a model that closely mimics the complexities of human cancer biology, leading to more accurate and reliable preclinical studies.

Materials and methods

Cell culture and reagents

The Vietnam breast cancer cell line number 1 (VNBRCA1) was kindly provided by the Laboratory of Stem Cell Research and Application at the University of Science (Ho Chi Minh, Vietnam) [18]. The VNBRCA1 cell line was cultured in Dulbecco's Modified Eagle Medium high glucose (Sigma-Aldrich), supplemented with 10% fetal bovine serum (Gibco), 1% penicillin/streptomycin antibiotics (Sigma-Aldrich) at 37 °C in a humidified 5 %CO_2. The morphology of VNBRCA1 cells was observed using an inverted phase-contrast microscope (Carl Zeiss Microscopy, LLC).

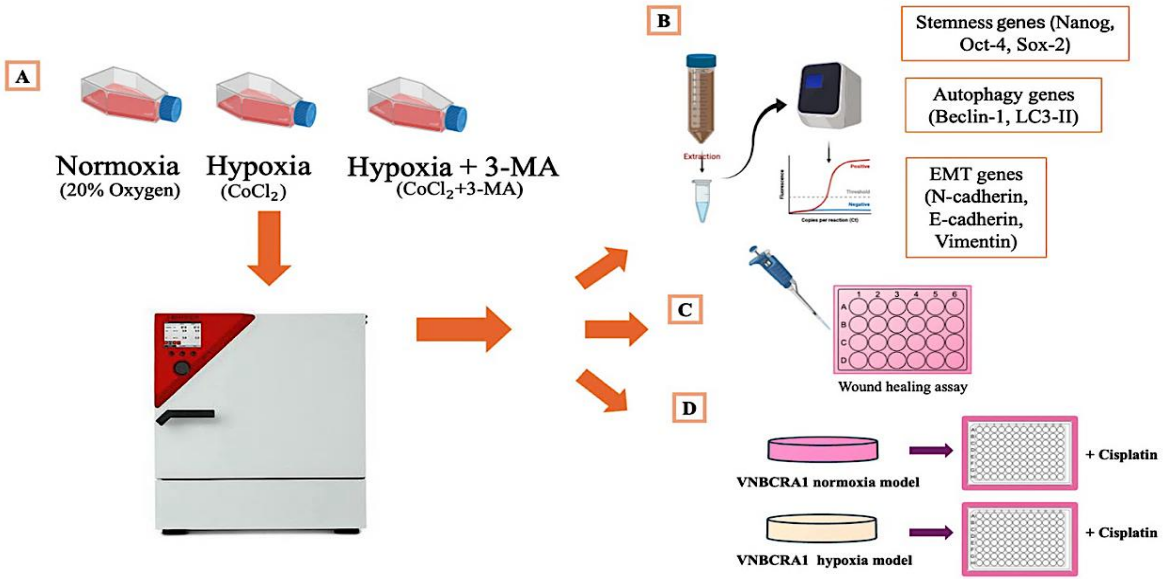

Figure 1 The experimental workflow is detailed as follows: (A) VNBRCA1 cells were cultured under 3 different conditions: normoxia (20 %O_2), hypoxia-mimicking conditions ($CoCl_2$), and hypoxia in combination with autophagy inhibition using 3-Methyladenine ($CoCl_2$ + 3-MA). Subsequently, these conditions were evaluated for (B) the expression levels of stemness-related genes, autophagy-related genes, and markers of EMT using RT-qPCR; (C) cell migration was assessed through both a wound healing assay and an Alamar Blue assay. Additionally, (D) a comparative analysis was performed by treating both normoxic and hypoxic VNBRCA1 models with cisplatin, followed by an evaluation of cell viability utilizing the Alamar Blue assay.

Cytotoxicity of $CoCl_2$ and 3-methyladenine (3-MA) on VNBRCA1 by alamar blue assay

VNBRCA1 cells (5×10^3) were seeded in 96-well plates (SPL, Korea) with a volume of 100 µL per well and cultured in a humidified incubator at 37 °C with 5 %CO_2 for 24 h. Following this incubation, $CoCl_2$ and 3-MA were added at varying concentrations, resulting in final concentrations of 0, 250, 300, 500, 750, and 1000 µM for $CoCl_2$, and 0, 2, 5, and 10 mM for 3-MA. The cytotoxic effects of $CoCl_2$ and 3-MA on VNBRCA1 were evaluated using the Alamar Blue assay. Specifically, Alamar Blue (Thermo Fisher Scientific, USA) was introduced to each well and then incubated at 37 °C with 5 %CO_2 for 30 min. After incubation, the optical density was measured at 595 nm (OD 595 nm) using a DTX880 machine (Beckman Coulter, USA).

Wound healing assay

Three cell culture models were seeded into a 6-well culture dish to create a monolayer. Once the cells reached approximately 80% confluence, a 200 µL sterile pipette tip was used to scratch the center of the

monolayer. Following this, the cells were washed with 1 mL of phosphate-buffered saline (PBS) to eliminate cell debris and to smooth the edges of the scratch. The culture plate was subsequently refreshed with 2 mL of fresh culture medium, supplemented with 10% fetal bovine serum (FBS), and incubated at 37 °C for 24 h. This serum concentration was selected based on prior studies that demonstrated effective migration analysis at this level [19]. Images were captured at 0 and 24 h using an inverted microscope from Carl Zeiss Microscopy, LLC. The analysis of the cell migration area was conducted using ImageJ software.

Reverse transcription quantitative real-time PCR (RT-qPCR)

RT-qPCR was conducted to quantitatively assess the changes in the expression of specific genes associated with hypoxic conditions (*HIF-1α and HIF-2α*), EMT markers (*E-cadherin, N-cadherin, Vimentin*), autophagy markers (*LC3-II and Beclin-1*), and stemness markers (*Nanog, Oct-4, Sox-2*). Total RNA was extracted from the samples using the Easy Blue Total RNA Extraction Kit (iNtRON Biotechnology, Korea), following the manufacturer's instructions. Quantitative RT-PCR was performed with the Luna® Universal 1-Step RT-qPCR Kit (Bio Labs, New England), utilizing a real-time PCR machine (Eppendorf, Hamburg, Germany). The thermal cycling conditions were established as follows: Reverse transcription was conducted at 55 °C for 10 min, followed by an initial denaturation at 95 °C for 1 min. This was followed by 40 cycles of denaturation at 95 °C for 10 s and annealing/extension at 60 °C for 30 s. A melt curve analysis was performed to confirm amplification specificity. The gene-specific primers are provided in **Table 1**. All primers were sourced from PHUSA Biochem, Vietnam. The RT-qPCR data were normalized and quantified using the $2^{-\Delta\Delta Ct}$ method, with *β-actin* serving as the reference control.

Table 1 Primer sequences used in RT-qPCR.

Gene	Primer	References
HIF-1α	Forward: 5' TGGTGACATGATTTACATTTCTGA 3' Reverse: 5' AAGGCCATTTCTGTGTGTAAGC 3'	[20]
HIF-2α	Forward: 5′ GTCTCTCCACCCCATGTCTC 3′ Reverse: 5′ GGTTCTTCATCCGTTTCCAC 3′	[21]
E-cadherin	Forward: 5' GACGCCATCAACACCGAGTT 3' Reverse: 5' CTTTGTCGTTGGTTAGCTGGT 3'	[22]
N-cadherin	Forward: 5' GACGCCATCAACACCGAGTT 3' Reverse: 5' CTTTGTCGTTGGTTAGCTGGT 3'	[22]
Vimentin	Forward: 5' GACGCCATCAACACCGAGTT 3' Reverse: 5' CTTTGTCGTTGGTTAGCTGGT 3'	[22]
LC3-II	Forward: 5' TGTCCGACTTATTCGAGAGCAGCA 3' Reverse: 5' TTCACCAACAGGAAGAAGGCCTGA 3'	[23]
Beclin-1	Forward: 5' ATGCAGGTGAGCTTCGTGTG 3' Reverse: 5' CTGGGCTGTGGTAAGTAATGGA 3'	[24]
Oct-4	Forward: 5' GAGGCAACCTGGAGAATTTGTTCC 3' Reverse: 5' ATGTGGCTGATCTGCTGCAGTG 3'	[25]
Sox-2	Forward: 5' CATCACCCACAGCAAATGACAGC 3' Reverse: 5' TTGCGTGAGTGTGGATGGGATTG 3'	[25]
Nanog	Forward: 5' TAGCAATGGTGTGACGCAGAAG 3' Reverse: 5' TCTGGTTGCTCCACATTGGAAGG 3'	[25]
β-actin	Forward: 5' CTGGAACGGTGAAGGTGACA 3' Reverse: 5' AAGGGACTTCCTGTAACAACGCA 3'	[26]

Impact of cancer drug (Cisplatin) on the cancer model

VNBRCA1 cells (5×10^3) were seeded at a volume of 100 µL per well in 96-well plates (SPL, Korea) and cultured in a humidified incubator at 37 °C with 5 %CO_2 for 24 h. Subsequently, 10 µL of CoCl2 was added to each well to establish hypoxic conditions. Both normoxic and hypoxic models were treated with differing concentrations of cisplatin (PHR1624-200MG, Sigma Aldrich), ranging from 0 to 100 µM (0, 20, 40, 60, 80, 100 µM) for 24 h. The proliferation of VNBRCA1 was assessed at 24 h using the Alamar Blue assay.

Statistical analysis

GraphPad Prism software (GraphPad Software Inc., USA) was employed to analyze the experimental data. All data were presented as the mean ± standard deviation (SD) of independent triplicate experiments. Multiple T-tests or one-way analyses of variance (ANOVA) were used to compare between groups. Student's t-test was used to determine the significance of all pairwise comparisons of interest. A statistically significant difference was considered when $p < 0.05$.

Results and discussion

Optimization of the hypoxic conditions using various concentrations of $CoCl_2$

In this study, VNBRCA1 cells were exposed to different concentrations of $CoCl_2$ ranging from 0 to 1000 µM for 24 h to evaluate their cytotoxicity. The results showed no significant differences between the concentrations at 24 h, particularly at 250 µM (**Figure 2(A)**). Hence, $CoCl_2$ concentrations ranging from 0 to 1000 µM were considered non-toxic at 24 h and suitable for further experiments.

$CoCl_2$ has been widely employed as a chemical inducer of hypoxia, as it stabilizes the hypoxia-inducible factor proteins, particularly HIF-1α and HIF-2α. Under normoxic conditions, hypoxia-inducible factor undergoes rapid degradation via the ubiquitin-proteasome pathway. However, the presence of $CoCl_2$ inhibits this degradation, resulting in the accumulation of *HIF-1α* and *HIF-2α* [27]. In this study, we systematically evaluated the effects of $CoCl_2$ concentrations ranging from 0 to 1000 µM on the expression of *HIF-1α* and *HIF-2α* in Vietnamese breast cancer cells (VNBRCA1) to determine the optimal condition for hypoxia simulation. Our results demonstrate that 250 µM $CoCl_2$ significantly increased the expression of *HIF-1α* compared to all other concentrations (0, 100, 300, 500, 750, and 1000 µM), except 200 µM. Although the difference between 200 µM and 250 µM was not statistically significant, the expression level of *HIF-1α* was notably higher at 250 µM. This finding suggests that 250 µM might be the optimal concentration for inducing *HIF-1α* expression in VNBRCA1. Regarding *HIF-2α*, 250 µM $CoCl_2$ led to a significant increase in expression compared to 100 µM and 200 µM; however, no significant differences were observed with higher concentrations (300, 500, 750, and 1000 µM) (**Figure 2(B)**). Consequently, 250 µM $CoCl_2$ was identified as the optimal concentration for simulating hypoxic conditions in VNBRCA1 cell lines, demonstrating significant effects on both *HIF-1α* and *HIF-2α* while remaining relatively safe for *in vitro* studies. Notably, microscopic examination of VNBRCA1 cells treated with 250 µM $CoCl_2$ showed normal growth and the preservation of typical cell morphology observed under normoxic conditions (**Figures 2(C) - 2(D)**). These results are consistent with previous reports on $CoCl_2$-mediated *HIF* stabilization and confirm its efficacy in inducing a hypoxic response [27]. Consequently, 250 µM $CoCl_2$ was selected for further investigation of the downstream analysis of hypoxia on key cancer hallmarks, including autophagy, stemness, and cell migration.

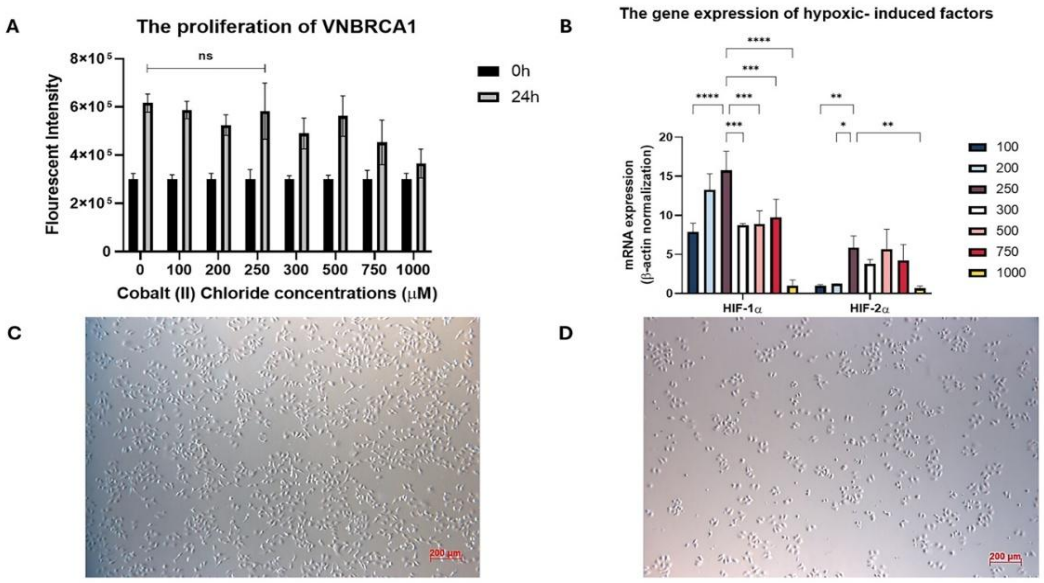

Figure 2 Optimize $CoCl_2$ concentration to induce hypoxia. (A) VNBRCA1 proliferation after 24 h, and (B) expression of hypoxic-related genes *HIF-1α* and *HIF-2α* at $CoCl_2$ concentrations from 0 - 1000 μM (*$p < 0.05$, ** $p < 0.01$, *** $p < 0.001$, ****$p < 0.0001$). The cell morphology was captured under normoxic (C), and hypoxic conditions (D).

Assessment of 3-MA cytotoxicity and its autophagy inhibition in VNBRCA1 cells

The VNBRCA1 cells were treated with concentrations of 0 mM, 5 mM, and 10 mM of 3-MA for 24 h to evaluate the drug's toxicity. The results showed no significant differences among these concentrations. However, cell proliferation slightly decreased at the 24-h mark in the 5 and 10 mM treatment groups compared to the non-treated. Therefore, the range of 3-MA concentrations from 0 to 10 mM at the 24-hour mark was considered safe for subsequent experiments (**Figure 3(A)**). Since there was no significant impact on the cancer cells, the 5 mM concentration of 3-MA was chosen for further experiments to minimize drug usage while ensuring safety.

3-MA is a well-known autophagy inhibitor, inhibiting autophagy by inhibiting class III phosphatidylinositol 3-kinase (PI3K) [28]. To assess the effectiveness of 3-MA in autophagy suppression, RT-qPCR was performed on VNBRCA1. VNBRCA1 cells were either pretreated with 5 mM 3-MA or left untreated. The gene expression of autophagy-related genes (*LC3-II, Beclin-1*) and hypoxia-related genes (*HIF-1α, HIF-2α*) under the influence of 3-MA was evaluated. As a result, the gene expression of the *HIF-1α* treated with 3-MA decreased in comparison with those not treated (p-value ≤ 0.05). Especially, the hypoxic-related genes (*HIF-2α*) and autophagy-related gene (*LC3-II*) treated with 3-MA showed a significant difference compared to the untreated group (p-value ≤ 0.01). *Beclin-1*, an autophagy-related gene, exhibited a reduction in gene expression; however, this difference was not statistically significant when compared to the control group (**Figure 3(B)**). Therefore, 3-MA (5 mM) is the suitable concentration for conducting the next experiment due to its ability to reduce autophagy properties and non-toxicity to the VNBRCA1.

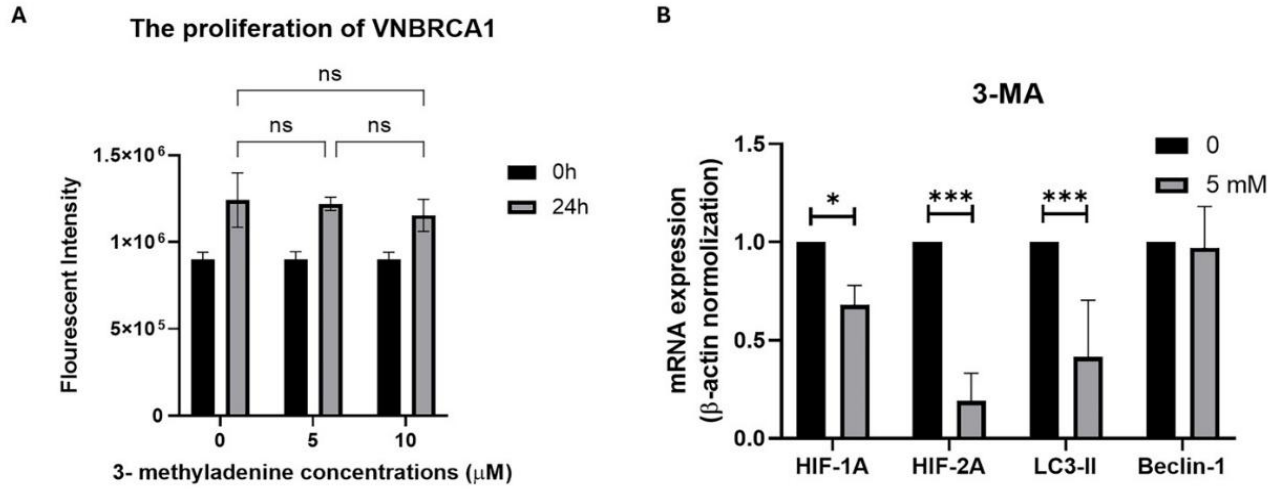

Figure 3 (A) A cytotoxicity assessment of 3-MA on VNBRCA1 growth, (B) RT-qPCR results to evaluate the expression of autophagy-related genes and hypoxia-related genes under 3-MA (*$p < 0.05$, *** $p < 0.001$).

Analysis of autophagy and stemness gene expression under hypoxic conditions

To investigate the effects of hypoxia models on downstream cancer hallmarks such as autophagy and stemness, VNBRCA1 cells were treated with $CoCl_2$ and 3-MA. Analysis of cell viability demonstrated that neither 250 μM $CoCl_2$ nor 5 mM 3-MA inhibited cell proliferation after 24 h of treatment (**Figures 3(A) - 4(A)**), thereby allowing for further molecular analysis free from the confounding effects of cytotoxicity. Gene expression analysis revealed that $CoCl_2$ significantly upregulated hypoxia-related genes (*HIF-1α, HIF-2α*) and autophagy-associated genes (*LC3-II, Beclin-1*), while 3-MA effectively inhibited the expression of autophagy genes (**Figures 2(B) - 3(B)**). The VNBRCA1 was thereafter cultured in 3 different models, including normoxia (without any treatment), hypoxia (supplemented with $CoCl_2$), and hypoxia supplemented with 3-MA (supplemented with $CoCl_2$ + 3-MA) to examine the autophagy gene expression in hypoxic conditions. Interestingly, as the expression of *HIF-1α* and *HIF-2α* increased, the autophagy-related gene (*LC3-II, Beclin-1*) also showed considerable growth. Specifically, the expression of *HIF-1α* and *HIF-2α* under hypoxia increased dramatically, being approximately 3 and 2 times higher than normoxia (p-value ≤ 0.0001). This finding aligns with previous reports demonstrating that hypoxia promotes autophagy as an adaptive survival mechanism in cancer cells under metabolic stress [11]. However, the pretreatment with the autophagy inhibitor 3-MA changed that gene expression completely. The *HIF-1α* and *HIF-2α* dropped considerably when treated with 3-MA in hypoxic conditions. While *HIF-1α* levels decreased to nearly match those of normoxia, *HIF-2α* levels were reduced 17 times compared to hypoxic conditions (p-value ≤ 0.0001). Additionally, the expression of the autophagy gene via *LC3-II* (p-value ≤ 0.0001) and *Beclin-1* gene (p-value ≤ 0.0001) in the hypoxic condition increased compared to those in the normoxic condition. On the other hand, the gene expression of *LC3-II* and *Beclin-1* had a significant decrease after being treated with 3-MA in hypoxic conditions, about 20 times (p-value ≤ 0.0001) and 2 times, respectively (**Figure 4(A)**). These results demonstrate a direct relationship between hypoxia and the activation of autophagy, as illustrated in **Figure 7**.

Further evaluation of stemness gene expression showed that hypoxia significantly increased the expression of *Nanog, Oct-4*, and *Sox-2* compared to normoxia, indicating the acquisition of stem cell-like properties. The expression of the stemness gene increased drastically in hypoxic conditions, yet was reduced when supplemented with 3-MA. In particular, the results showed that the expression of *Nanog, Oct-4,* and *Sox-2* increased in the hypoxic condition in comparison with those in the normoxic condition. Remarkably, the 2 genes *Oct-4* and *Sox-2* in the hypoxic condition demonstrated substantial growth compared to normoxia, about 441 times and 187 times (p-value ≤

0.0001), respectively (**Figure 4(B)**). This result reinforces the hypothesis that hypoxia promotes cancer stemness characteristics [29]. Intriguingly, the expressions of all 3 stemness genes started to reduce after being treated with 3-MA in the hypoxic condition, underscoring the connection between autophagy and stemness in breast cancer cells (**Figure 7**).

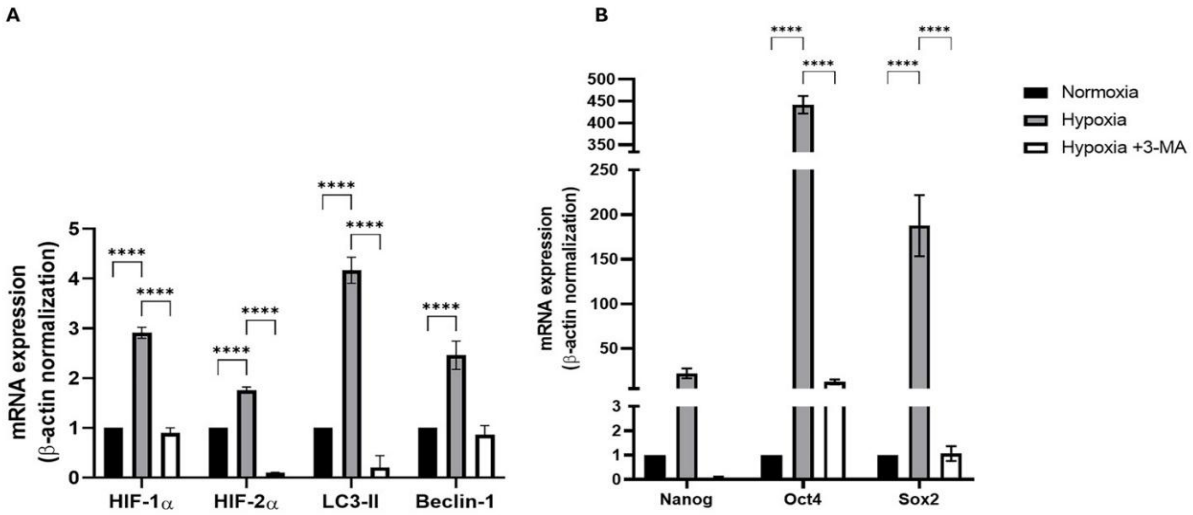

Figure 4 Evaluation of the gene expression of (A) Autophagy and hypoxia marker and (B) Stemness marker of VNBRCA1 under 3 different models (****$p < 0.0001$).

Evaluation of EMT-related gene expression and migration ability in VNBRCA1 cells

EMT is a crucial process in cancer progression, especially in facilitating metastasis. To assess EMT in VNBRCA1 cells, we conducted both a wound healing assay (to evaluate migratory capacity) and RT-qPCR (to measure the expression of EMT-related genes) under 3 distinct conditions; normoxia, hypoxia (induced by $CoCl_2$ treatment), and hypoxia supplemented with 3-MA. The result interestingly showed that the hypoxia exhibited the top migration compared to hypoxia+3-MA and normoxia. The hypoxia supplement with 3-MA showed a lower migration rate compared to hypoxia as well, yet still higher than that of normoxia. Specifically, the wound healing ability of normoxia, hypoxia, and hypoxia treated with 3-MA is 46.36% ± 3.3%, 73.37% ± 2.69%, and 62.53% ± 2.74%, respectively. The area of wound healing expanded around 1.5 times in hypoxic conditions (p-value ≤ 0.001) compared to the normoxic condition, proving that $CoCl_2$-mediated hypoxia also significantly enhanced cell migration. Furthermore, the wound healing area was reduced in size by approximately 1.17 times (p-value ≤ 0.05) after being treated with 3-MA in a hypoxic condition. Additionally, the wound healing area under hypoxia supplemented with 3-MA showed significant differences in healing ability compared to normoxic conditions, approximately 1.3 times greater (p-value < 0.01) (**Figures 5(A) - 5(B)**). These results highlight the importance of autophagy in promoting cell migration during hypoxic stress, indicating that autophagy may serve as a mediator of EMT (**Figure 7**).

For further evaluation of the EMT at the molecular level, the gene expression of EMT markers, including *E-cadherin, N-cadherin*, and *Vimentin*, was quantified in 3 different models by RT-qPCR. Unexpectedly, all 3 genes, *E-cadherin, N-cadherin,* and *Vimentin,* were upregulated under hypoxic conditions. More specifically, the expression of *E-cadherin* in hypoxic conditions had a 30-fold increase compared to that of normoxia (p-value ≤ 0.0001). Interestingly, the results indicated a significant increase in both mesenchymal (such as *N-cadherin* and *Vimentin*) and epithelial (*E-cadherin*) expression under hypoxic conditions. This finding contradicts the established hypothesis that EMT involves the downregulation of E-cadherin alongside the upregulation of *Vimentin* and *N-cadherin.* This emerging evidence suggests that instead of a complete EMT, a "hybrid" EMT may play a crucial role in this process. Hybrid EMT, characterized by simultaneous

expression of both epithelial and mesenchymal traits, may confer advantages for survival and adaptation in challenging hypoxic environments. Furthermore, hybrid EMT can enhance cellular plasticity, facilitate collective migration, promote cancer stemness, contribute to drug resistance, and enhance metastasis in cancer [30]. Similarly, the reduction of 3 gene expressions was recorded after treating with 3-MA in a hypoxic condition (**Figure 5(C)**), further implicating autophagy as a regulator of hybrid EMT. The results from both EMT gene expression and migration assessment suggest that hypoxia-induced autophagy contributes to a hybrid EMT phenotype in VNBRCA1 cells**,** enhancing their migratory potential, and this effect can be partially reversed by autophagy inhibition. A schematic model summarizing these interrelated pathways is illustrated in **Figure 7**.

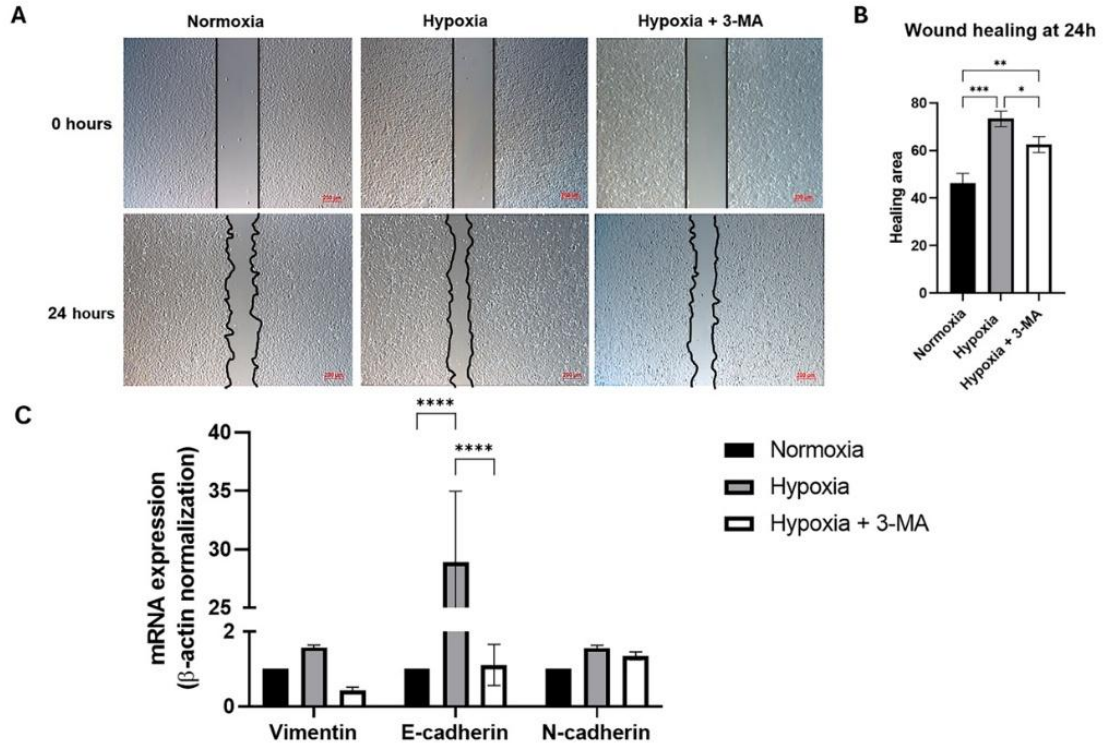

Figure 5 (A) Images, (B) chart illustrating the migratory ability (*p <0.05, ** p < 0.01, *** p < 0.001), and (C) RT-qPCR results from migration-related genes (****p < 0.0001) of VNBRCA1 under 3 distinct conditions.

Assessment of cisplatin sensitivity in hypoxia-induced VNBRCA1 cells

After examining the characteristics of cancer, including hypoxia, autophagy, and migration, we evaluated the impact of a chemotherapeutic drug, cisplatin, on the hypoxic-induced VNBRCA models compared to the normoxic conditions. As the concentration of cisplatin increased, there were no significant differences in proliferation between normoxia and hypoxia across various concentrations, including 0, 20, 40, 60, 80, and 100 μM. Notably, there was higher cell proliferation under hypoxic conditions than under normoxic conditions at Cisplatin concentrations of 40, 60, and 80 μM. The drug effects on both models were almost the same, and there was no statistically significant difference between hypoxic and normoxic conditions (**Figure 6(B)**). This finding highlights the model's capability to demonstrate similar cell rates as the normoxic condition when exposed to cancer drugs. Furthermore, the hypoxic model offers a more accurate representation of the tumor microenvironment, as evidenced by the induction of key cancer hallmarks, including autophagy, EMT, and stemness (**Figure 7**). Morphological analysis of hypoxic cells treated with cisplatin further corroborates this observation. These cells exhibited an elongated, spindle-like shape typically associated with a mesenchymal phenotype, indicating the presence of EMT features

under hypoxic stress (**Figure 6(A)**). This morphological transformation provides robust evidence that hypoxia may enhance EMT, which is a well-established contributor to drug resistance, metastasis, and unfavorable clinical outcomes.

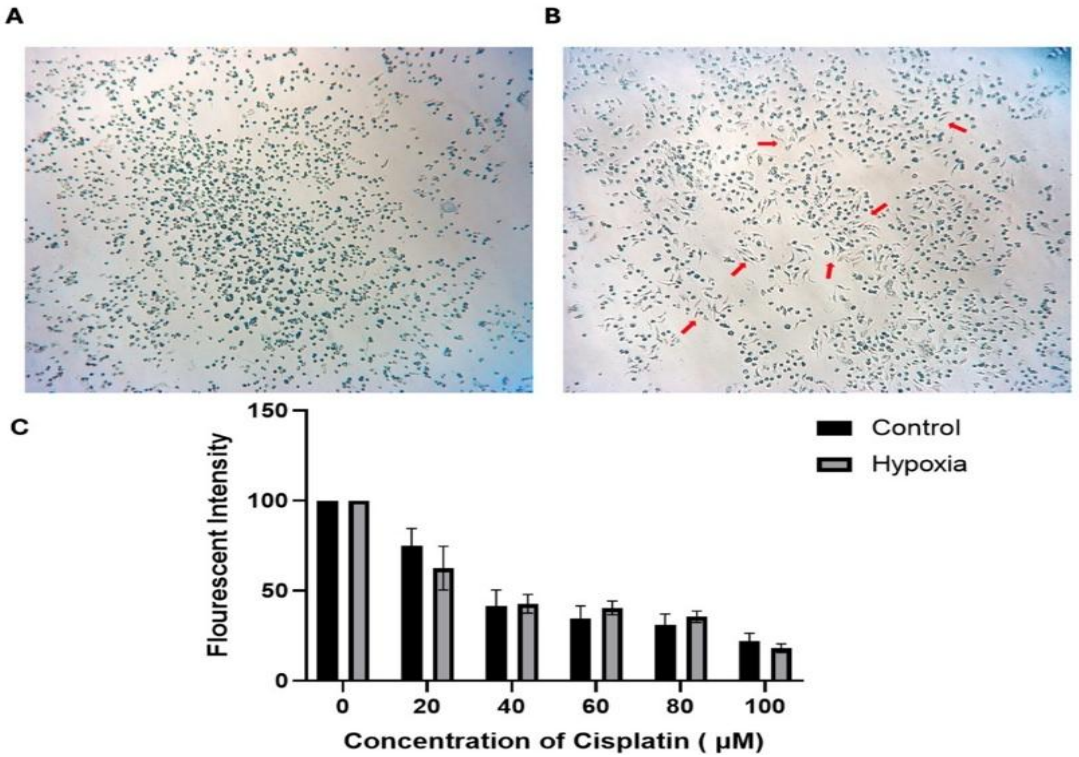

Figure 6 Images of VNBRCA1 demonstrating the effects of 60 μM Cisplatin in traditional (A) and hypoxia models (B). The proliferation of VNBRCA1 under the influence of Cisplatin in both traditional and hypoxia models (C).

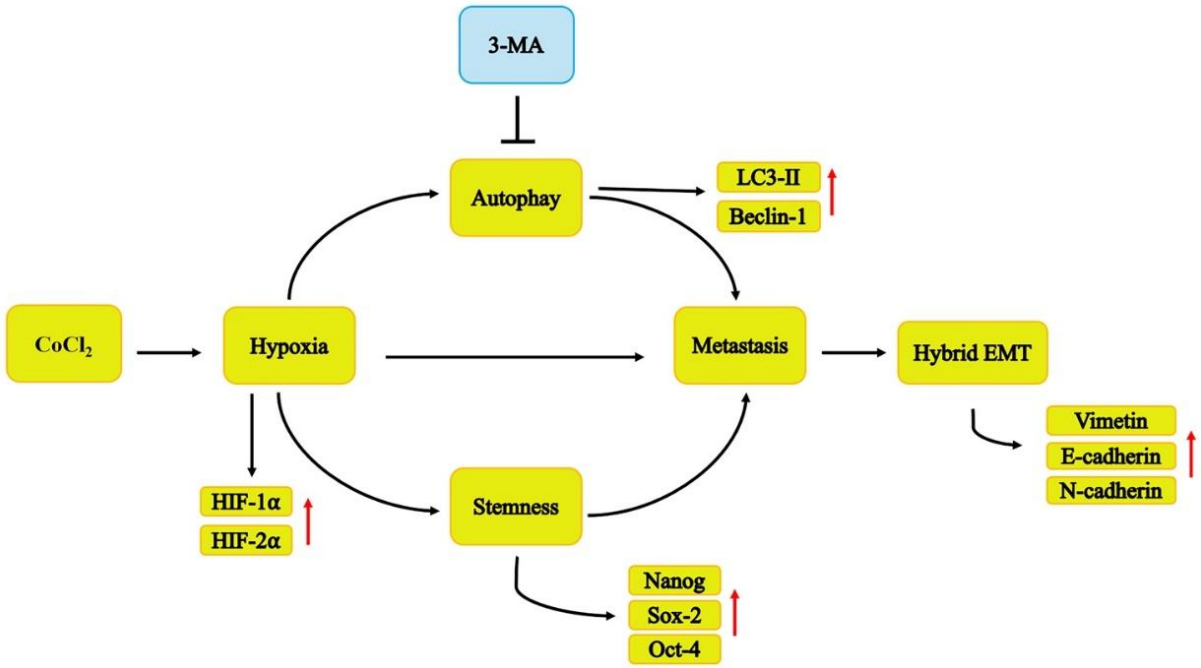

Figure 7 The schematic representation of the correlation between hypoxia, autophagy, stemness, and metastasis in VNBRCA1 cells.

Table 2 Comparative analysis of *in vitro* hypoxia models.

Criteria	$CoCl_2$-Based 2D model	Hypoxia chamber (2D)	3D spheroid under hypoxia	DFO (Deferoxamine)
Mechanism of Hypoxia Induction	Chemical HIF-1α/2α stabilization via prolyl hydroxylase inhibition	Physical reduction of ambient O_2	O_2 diffusion limitation in spheroids	Iron chelation blocks HIF degradation
Mimics Tumor O_2 Microenvironment	Mimics pseudohypoxia rather than true oxygen depletion	Mimics chronic hypoxia through sustained low oxygen exposure	Closely replicates oxygen gradients present in solid tumors	Provides partial mimicry through transient HIF stabilization
Cost & Equipment	Very low cost, no specialized equipment required	High cost; requires sealed chambers and gas cylinders	Moderate to high; necessitates ECM scaffolds or low-adhesion plates	Low cost
Ease of Use	Simple	Requires technical setup and environmental monitoring	Demands expertise in 3D culture techniques	Easy to apply
O_2 Gradient Simulation	None (uniform chemical hypoxia)	Limited (unless multilayered)	Yes – via diffusion gradients in 3D structure	None
HIF-1α / 2α Induction	Robust and dose-dependent induction	High and regulated by O_2 tension	High induction in spheroid core; lower at periphery	Moderate and transient activation
Downstream Pathways Activated	Hypoxia, stemness, EMT, autophagy, cisplatin resistance	HIF targets gene expression	EMT, necrosis, metabolic reprogramming	Primarily HIF-dependent pathways
Reproducibility	High (easy to control dose, batch-to-batch consistency)	Moderate (depends on O_2 stability)	Variable (spheroid uniformity varies)	Moderate
Advantages	• Simple, reproducible, and cost-effective • Rapid HIF-1α/2α induction • Suitable for drug screening and short-term hypoxia studies	Appropriate for chronic hypoxia modeling	• Replicates physiological oxygen levels • Closely resembles *in vivo* tumor architecture	• Easy and inexpensive chemical methodInduces HIF-1α
Disadvantages	• Pseudohypoxia (not real O_2 decrease). • May not capture the intermediate hypoxia.	• High cost • Requires hypoxia chambers and gas control • Uneven hypoxic environment • May not fully recapitulate tumor microenvironments	• Labor-intensive • Variability in spheroid size and oxygen diffusion	• Non-specific effects due to iron metabolism
References	This work	[31, 32]	[32-34]	[35, 36]

A range of *in vitro* hypoxia models has been developed to mimic the diverse oxygenation profiles observed in solid tumors, as illustrated in **Table 2**. Among these, the $CoCl_2$-based 2D model utilized in this study is distinguished by its simplicity, reproducibility, and cost-effectiveness. This model chemically stabilizes HIF-1α and HIF-2α by inhibiting prolyl hydroxylase activity, facilitating the rapid, dose-dependent activation of hypoxia-related pathways, including EMT, oxidative stress, autophagy, and cisplatin resistance—key features relevant to tumor progression and therapy resistance. Unlike models that require intricate instrumentation or extensive culturing protocols, the $CoCl_2$ approach does not necessitate specialized equipment, and its straightforward add-and-incubate format renders it ideal for high-throughput drug screening and short-term investigations of hypoxic stress. Additionally, it ensures high reproducibility and provides precise control over the level and duration of HIF activation, which is crucial for conducting mechanistic studies. Although it does not reduce ambient oxygen levels and thus models pseudohypoxia rather than true hypoxic conditions, its high reproducibility, cost-efficiency, and operational simplicity make it particularly attractive for rapid screening and mechanistic studies in cancer research.

In contrast, the hypoxia chamber model involves a controlled reduction of atmospheric oxygen, allowing for a more physiologically relevant exposure to chronic hypoxia. This model provides precise regulation of oxygen tension and sustained activation of HIF, making it suitable for long-term studies. However, it necessitates the use of sealed incubators, gas cylinders, and continuous environmental monitoring, leading to high costs and limited accessibility, particularly in resource-constrained laboratories. Additionally, the uniform oxygen exposure in 2D monolayers may not adequately reflect the oxygen gradients seen in solid tumors [31, 32]. The 3D spheroid model under hypoxic conditions is noteworthy for its capacity to naturally create oxygen diffusion gradients, closely mimicking the heterogeneity of the tumor microenvironment. Within the spheroid core, cells experience severe hypoxia or even necrosis, while those at the periphery remain relatively normoxic. This gradient formation facilitates the examination of spatially resolved responses to hypoxia, including metabolic zoning and differential drug sensitivity. Nonetheless, this approach is labor-intensive, demands proficiency in 3D culture techniques, and is subject to variability in spheroid size and morphology, which can limit reproducibility and scalability [32-34]. DFO, a chemical mimetic of hypoxia, induces HIF stabilization by chelating intracellular iron, thereby preventing the degradation of HIF-1α. While it is easy to apply and cost-effective, the effects of DFO are often transient and less specific, as it may interfere with other iron-dependent cellular processes. Thus, it provides only a partial mimicry of hypoxia and may not be the best choice for studies requiring sustained or spatially defined hypoxic conditions [35, 36]. In summary, while no model completely captures all facets of tumor hypoxia, the $CoCl_2$-based model utilized in this study strikes a commendable balance between practicality, consistency, and biological relevance. This model is particularly advantageous for investigations focused on acute hypoxic responses and drug resistance mechanisms, offering a robust and efficient alternative. Although it does not replicate the true oxygen gradients or intermediate hypoxia levels observed in other research [37], its experimental benefits position it as a valuable primary model in the field of hypoxia research.

In conclusion, this study has successfully developed a straightforward yet highly effective model for VNBRCA1, capturing essential features of the tumor microenvironment such as hypoxia, autophagy, EMT, stemness, and drug response. These results underscore the model's promise for advancing our understanding of tumor biology and for crafting therapeutic strategies specifically designed for the hypoxic tumor microenvironment.

Conclusions

This study demonstrates the utility of using $CoCl_2$ as an effective tool to mimic and enhance hypoxia in a 2D breast cancer model. By evaluating the optimal $CoCl_2$ concentrations, the researchers were able to induce a robust hypoxic response, as evidenced by the increased expression of key hypoxia-related factors, such as *HIF-1α* and *HIF-2α*. Further investigation of the downstream effects of $CoCl_2$-induced hypoxia provided valuable insights into the tumor microenvironment,

revealing that $CoCl_2$-induced hypoxia promotes autophagy, enriches cancer stemness characteristics, and enhances migratory capabilities, likely through the activation of hybrid EMT. Moreover, although the model demonstrates comparable cell rates when exposed to Cisplatin, it aligns more closely with the intricacies of the tumor microenvironment than the traditional model. Overall, this study highlights the versatility, efficiency, and cost-effectiveness of the $CoCl_2$-mediated hypoxia model in recapitulating the key aspects of the tumor microenvironment, paving an *in vitro* platform to evaluate the efficacy of therapeutic interventions and developing more effective anti-cancer strategies.

Acknowledgements

This research is funded by University of Science, Vietnam, VNU-HCM under grant number T2024-82.

Declaration of Generative AI in Scientific Writing

The authors acknowledge the use of generative AI tools (e.g., ChatGPT by OpenAI) during the preparation of this manuscript. These tools were used exclusively for language editing and grammar correction. No AI tools were used for content generation, data analysis, or interpretation. The authors take full responsibility for the integrity, originality, and conclusions of this work.

CRediT Author Statement

Pham Duy Khuong: Data curation, Methodology, Project administration, Resources, Supervision, Validation, Visualization, and Writing – original draft.

Chau Nguyen Minh Hoang: Methodology, Data curation, Formal analysis, Validation, Visualization, and Writing – original draft.

Bui Dinh Khan: Data curation, Validation, and Resources.

Ngo The Tran Nhan: Data curation, and Validation.

References

[1] F Bray, M Laversanne, H Sung, J Ferlay, RL Siegel, I Soerjomataram and A Jemal. Global cancer statistics 2022: GLOBOCAN estimates of incidence and mortality worldwide for 36 cancers in 185 countries. *CA: A Cancer Journal for Clinicians* 2024; **74(3)**, 229-263.

[2] CH Wong, KW Siah and AW Lo. Estimation of clinical trial success rates and related parameters. *Biostatistics* 2019; **20**, 273-286.

[3] R Dave, K Pandey, R Patel, N Gour and D Bhatia. Leveraging 3D cell culture and AI technologies for next-generation drug discovery. *Cell Biomaterials* 2025; **1**, 100050.

[4] IR Powley, M Patel, G Miles, H Pringle, L Howells, A Thomas, C Kettleborough, J Bryans, T Hammonds, M MacFarlane and C Pritchard. Patient-derived explants (PDEs) as a powerful preclinical platform for anti-cancer drug and biomarker discovery. *British Journal of Cancer* 2020; **122**, 735-744.

[5] M Turetta, FD Ben, G Brisotto, E Biscontin, M Bulfoni, D Cesselli, A Colombatti, G Scoles, G Gigli and LLD Mercato. Emerging technologies for cancer research: Towards personalized medicine with microfluidic platforms and 3D tumor models. *Current Medicinal Chemistry* 2018; **25(35)**, 4616-4637.

[6] MA Barbosa, CP Xavier, RF Pereira, V Petrikaitė and MH Vasconcelos. 3D cell culture models as recapitulators of the tumor microenvironment for the screening of anti-cancer drugs. *Cancers* 2021; **14**, 190.

[7] H Ruiz-Garcia, K Alvarado-Estrada, P Schiapparelli, A Quinones-Hinojosa and DM Trifiletti. Engineering three-dimensional tumor models to study glioma cancer stem cells and tumor microenvironment. *Frontiers in Cellular Neuroscience* 2020; **14**, 558381.

[8] A Baru, S Mazumdar, P Kundu, S Sharma, BPD Purakayastha, S Khan, Profile, R Gupta and NM Arora. Recapitulating tumor microenvironment using preclinical 3D tissueoids model for accelerating cancer research and drug screening. *BioRxiv* 2020; **21**, 423825.

[9] DA Barth, F Prinz, J Teppan, K Jonas, C Klec and M Pichler. Long-noncoding RNA (lncRNA) in the regulation of hypoxia-inducible factor (HIF) in cancer. *Non-coding RNA* 2020; **6**, 27.

[10] MZ Bakleh and AAH Zen. The distinct role of HIF-1α and HIF-2α in hypoxia and angiogenesis. *Cells* 2025; **14**, 673.

[11] RF Zaarour, B Azakir, EY Hajam, H Nawafleh, NA Zeinelabdin, AST Engelsen, J Thiery, C

Jamora and S Chouaib. Role of hypoxia-mediated autophagy in tumor cell death and survival. *Cancers* 2021; **13(3)**, 533.

[12] HR Yun, YH Jo, J Kim, Y Shin, SS Kim and TG Choi. Roles of autophagy in oxidative stress. *International Journal of Molecular Sciences* 2020; **21**, 3289.

[13] R Rakesh, LCP Dharshini, KM Sakthivel and RR Rasmi. Role and regulation of autophagy in cancer. *Biochimica et Biophysica Acta (BBA) - Molecular Basis of Disease* 2022; **1868**, 166400.

[14] D Ribatti, R Tamma and T Annese. Epithelial-mesenchymal transition in cancer: A historical overview. *Translational Oncology* 2020; **13**, 100773.

[15] I Akrida and H Papadaki. Adipokines and epithelial-mesenchymal transition (EMT) in cancer. *Molecular and Cellular Biochemistry* 2023; **478**, 2419-2433.

[16] SY Tam, VW Wu and HK Law. Hypoxia-induced epithelial-mesenchymal transition in cancers: HIF-1α and beyond. *Frontiers in Oncology* 2020; **10**, 486.

[17] C Su, J Zhang, Y Yarden and L Fu. The key roles of cancer stem cell-derived extracellular vesicles. *Signal Transduction and Targeted Therapy* 2021; **6**, 109.

[18] PV Phuc, TTT Khuong, LV Dong, TT Giang and PK Ngoc. Isolation and characterization of breast cancer stem cells from malignant tumours in Vietnamese women. *Journal of Cell and Animal Biology* 2010; **4(12)**, 163-169.

[19] S Prajapati, B Prajapati, M Patel and R Gupta. Acidic pH at physiological salinity enhances the antitumor efficacy of lenvatinib, a drug targeting vascular endothelial growth factor receptors. *World Academy of Sciences Journal* 2024; **6**, 63.

[20] S Chakraborty, A Adhikary, M Mazumdar, S Mukherjee, P Bhattacharjee, D Guha, T Choudhuri, S Chattopadhyay, G Sa, A Sen and T Das. Capsaicin-induced activation of p53-SMAR1 auto-regulatory loop down-regulates VEGF in non-small cell lung cancer to restrain angiogenesis. *Plos One* 2014; **9**, e99743.

[21] BC Jham, T Ma, J Hu, R Chaisuparat, ER Friedman, PP Pandolfi, A Schneider, A Sodhi and S Montaner. Amplification of the angiogenic signal through the activation of the TSC/mTOR/HIF axis by the KSHV vGPCR in Kaposi's sarcoma. *Plos One* 2011; **6(4)**, e19103.

[22] B Shi, C Ma, G Liu and Y Guo. MiR-106a directly targets LIMK1 to inhibit proliferation and EMT of oral carcinoma cells. *Cellular & Molecular Biology Letters* 2019; **24**, 1.

[23] C Morell, A Bort, D Vara-Ciruelos, A Ramos-Torres, M Altamirano-Dimas, I Diaz-Laviada and N Rodriguez-Henche. Up-regulated expression of LAMP2 and autophagy activity during neuroendocrine differentiation of prostate cancer LNCaP cells. *Plos One* 2016; **11(9)**, e0162977.

[24] R RK Ramakrishnan, K Bajbouj, SA Heialy, B Mahboub, AW Ansari, IY Hachim, S Rawat, L Salameh, MY Hachim, R Olivenstein, R Halwani, R Hamoudi and Q Hamid. IL-17 induced autophagy regulates mitochondrial dysfunction and fibrosis in severe asthmatic bronchial fibroblasts. *Frontiers in Immunology* 2020; **11**, 1002.

[25] CR Jeter, B Liu, X Liu, X Chen, C Liu, T Calhoun-Davis, J Repass, H Zaehres, JJ Shen and DG Tang. NANOG promotes cancer stem cell characteristics and prostate cancer resistance to androgen deprivation. *Oncogene* 2011; **30(36)**, 3833-3845.

[26] M Youssef, N Moussa, MW Helmy and M Haroun. Unraveling the therapeutic potential of GANT61/Dactolisib combination as a novel prostate cancer modality. *Medical Oncology* 2022; **39**, 143.

[27] D Xu and C Li. Regulation of the SIAH2-HIF-1 Axis by protein kinases and its implication in cancer therapy. *Frontiers in Cell and Developmental Biology* 2021; **9**, 646687.

[28] Q Bo, M Shen, M Xiao, J Liang, Y Zhai, H Zhu, M Jiang, F Wang, X Luo and X Sun. 3-Methyladenine alleviates experimental subretinal fibrosis by inhibiting macrophages and M2 polarization through the PI3K/Akt pathway. *Journal of Ocular Pharmacology and Therapeutics* 2020; **36(8)**, 618-628.

[29] R Mu, Y Zou, K Tu, D Wang, D Tang, Z Yu and L Zhao. Hypoxia promotes pancreatic cancer cell dedifferentiation to stem-like cell phenotypes with high tumorigenic potential by the HIF-1α/Notch

signaling pathway. *Pancreas* 2021; **50(5)**, 756-765.

[30] D Sinha, P Saha, A Samanta and A Bishayee. Emerging concepts of hybrid epithelial-to-mesenchymal transition in cancer progression. *Biomolecules* 2020; **10**, 1561.

[31] S Saxena, I Agrawal, P Singh and S Jha. Portable, low-cost hypoxia chamber for simulating hypoxic environments: Development, characterization and applications. *Medical Devices & Sensors* 2020; **3**, e10064.

[32] S Riffle and RS Hegde. Modeling tumor cell adaptations to hypoxia in multicellular tumor spheroids. *Journal of Experimental & Clinical Cancer Research* 2017; **36**, 102.

[33] K Klimkiewicz, K Weglarczyk, G Collet, M Paprocka, A Guichard, M Sarna, A Jozkowicz, J Dulak, T Sarna, C Grillon and C Kieda. A 3D model of tumour angiogenic microenvironment to monitor hypoxia effects on cell interactions and cancer stem cell selection. *Cancer Letters* 2017; **396**, 10-20.

[34] Y Liu, Z Mohri, W Alsheikh and U Cheema. The role of biomimetic hypoxia on cancer cell behaviour in 3D models: A systematic review. *Cancers* 2021; **13**, 1334.

[35] Y Zhang, MA Yapryntseva, A Vdovin, P Maximchik, B Zhivotovsky and V Gogvadze. Modeling hypoxia facilitates cancer cell survival through downregulation of p53 expression. *Chemico-Biological Interactions* 2021; **345**, 109553.

[36] Y Zhu, B Chang, Y Pang, H Wang and Y Zhou. Advances in Hypoxia-Inducible Factor-1α stabilizer deferoxamine in tissue engineering. *Tissue Engineering Part B: Reviews* 2022; **29**, 347-357.

[37] R Gupta, C Chetty, P Bhoopathi, S Lakka, S Mohanam, JS Rao and DE Dinh. Downregulation of uPA/uPAR inhibits intermittent hypoxia-induced epithelial-mesenchymal transition (EMT) in DAOY and D283 medulloblastoma cells. *International Journal of Oncology* 2011; **38(3)**, 733-744.